Geophysical Research Letters

RESEARCH LETTER
10.1029/2019GL086177

Physical Diagnosis of the 2016 Great Barrier Reef Bleaching Event

Kristopher B. Karnauskas[1,2]

[1]Department of Atmospheric and Oceanic Sciences, University of Colorado Boulder, Boulder, CO, USA, [2]Cooperative Institute for Research in Environmental Sciences, University of Colorado Boulder, Boulder, CO, USA

Key Points:
- A quantitative heat budget analysis of the 2016 marine heat wave in the Great Barrier Reef lights a path to large-scale climate processes
- The waning El Niño of 2015/2016 warmed regional seas with solar radiation; a terrestrial heat wave in Australia intensified coastal warming
- Long-term trends in marine and terrestrial records clarify role of global warming, widespread coral mortality in 2016 unlikely without it

Supporting Information:
- Supporting Information S1
- Movie S1

Correspondence to:
K. B. Karnauskas,
kristopher.karnauskas@colorado.edu

Citation:
Karnauskas, K. B. (2020). Physical diagnosis of the 2016 great barrier reef bleaching event. *Geophysical Research Letters*, *47*, e2019GL086177. https://doi.org/10.1029/2019GL086177

Received 12 NOV 2019
Accepted 4 MAY 2020
Accepted article online 18 MAY 2020

Abstract Widespread coral bleaching across the Great Barrier Reef (GBR) in 2016 is often reportedly caused by El Niño and/or global warming. However, the GBR is not in a region where it is straightforward to anticipate sea surface temperature (SST) warming during El Niño, and the role of climate change is unclear. This study uses a diverse range of observations to investigate the physical causes of SST anomalies that developed on the GBR in 2016. Warm SST anomalies developed in two stages. Initial warming was caused by El Niño shifting the global-scale pattern of convection, increasing solar radiation in the Coral Sea. The warm anomaly was extended and amplified near the coast by a terrestrial heat wave propagating across eastern Australia, further warming the GBR through turbulent heat flux. It is concluded that El Niño caused the SST anomaly, and global warming increased its amplitude and extended it by several months.

1. Introduction

Severe coral bleaching in the Great Barrier Reef (GBR) during 2016 has been extensively documented (Hughes et al., 2017, Hughes, Anderson, et al., 2018, Hughes, Kerry, et al., 2018; Great Barrier Reef Marine Park Authority, 2017), with estimates of coral mortality reaching two thirds of the northern GBR (ARC Centre of Excellence Coral Reef Studies, 2017) along with widespread ecosystem restructuring including declines in the diversity of reef fishes (Stuart-Smith et al., 2018). The sea surface temperature (SST) warming associated with the 2016 GBR bleaching event was characterized by two distinct warming pulses. Both pulses occurred following the peak of the 2015/2016 El Niño, and the strongest warming in the Coral Sea was concentrated along the coastline of northeastern Australia (Figure 1). Although the second warming pulse was beyond the typical austral summertime season when climatological SSTs are higher and corals are more susceptible to bleaching, repeat surveys of GBR corals would suggest that this extension of the marine heat wave hampered coral recovery. As reported in Hughes, Kerry, et al. (2018), many corals died between March and April 2016, but a delayed response was evident with further mortality reported in repeat surveys taken later in the year.

The 2016 bleaching event in the GBR is often reportedly associated with global warming and/or El Niño. However, the GBR is not in a region where it is straightforward to anticipate SST warming given an El Niño event (Lough, 1994; Zhang et al., 2017). Regardless of El Niño "flavor" (i.e., whether the maximum warming occurs in the central or eastern equatorial Pacific Ocean), the thermocline and SST variability in the far western tropical Pacific/Indo-Pacific region is weakly out of phase with the rest of the equatorial Pacific Ocean (see Figure 1 of Karnauskas, 2013). In fact, the contemporaneous correlation between El Niño–Southern Oscillation (ENSO) and SST anomalies in the GBR region is effectively zero (−0.06). Further analysis of this relationship reveals that ENSO explains at most 25% of the variance of SST anomalies in the GBR region, and only when the GBR lags ENSO by about 9 months and variability with periods shorter than about 1 year are filtered out (Figure S1 in the supporting information).

Despite the intense research and reporting on the severe marine ecosystem response, fundamentally lacking is a quantitative diagnosis of the climate processes leading to the 2016 marine heat wave in the GBR, guided by the physical controls on the ocean mixed layer temperature. The aim of this study is to shed light on why warm SST anomalies developed in the northwestern Coral Sea in 2016, including why they were concentrated along the northeastern coastline of Australia—essentially collocated with the GBR itself. The study begins with an ocean mixed layer heat budget analysis using almost exclusively satellite observations,

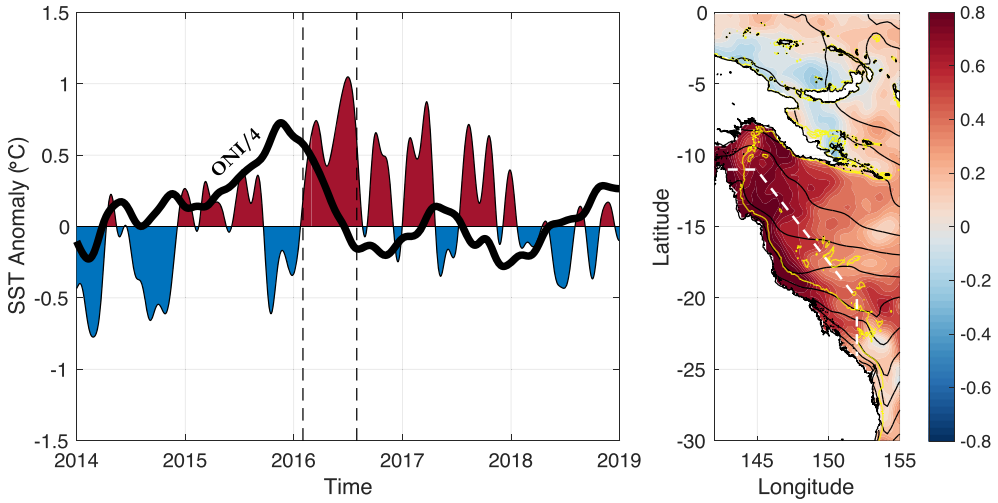

FIGURE 1. Left: Daily time series of SST anomaly (°C) in the GBR region (averaged over the domain marked by dotted white lines on the map) with a 60-day low-pass filter. Included is a time series of the Oceanic Niño Index (ONI) to represent ENSO variability, scaled by a factor of 0.25 to facilitate comparison. Right: Map of daily SST anomaly averaged from 1 February through 31 July 2016 (the time period marked with dashed black lines on the left). Also plotted are the 100-m isobath (yellow line) and February–July mean climatological SST isotherms (1982–2018 base period, contoured every 0.5°C, black lines).

followed by a broader diagnosis of the climatic phenomena leading to the observed perturbations to the GBR heat budget and a brief discussion of the role of climate variability and change in shaping the future of such marine ecosystems.

2. Data and Methods

Nine observational data sets are analyzed in this study, for the purposes of ocean mixed layer heat budget calculations and other diagnostic analyses of climate anomalies and trends. All data sets are gridded and global or near global. SST data sets include the NOAA High-Resolution Blended Analysis of Daily SST and Ice version 2 (OIv2, 1982–2018, daily, 0.25°) (Reynolds et al., 2002) and Hadley Centre Sea Ice and Sea Surface Temperature version 1 (1880–2018, monthly, 1°) (Rayner et al., 2003). The OIv2 data set was detrended prior to most analyses except for, of course, the analysis of trends that appears near the end of the paper (Figures 5 and S4). Surface or 2-m air temperature data sets include the ECMWF Reanalysis version 5 (ERA5, 1982–2018, monthly, 0.25°) (Hersbach et al., 2019) and the NASA GISS Surface Temperature Analysis version 4 (GISTEMP, 1880–2018, monthly, 2°) (Lenssen et al., 2019). Surface heat fluxes over the ocean are derived from INCOIS TropFlux version 1 (1982–2018, monthly, 1°) (Praveen Kumar et al., 2012), WHOI Objectively Analyzed Air-Sea Fluxes version 3 (OAFlux, 1982–2018, monthly, 1°) (Yu & Weller, 2007), and ERA5. Ocean mixed layer depth is derived from the IFREMER Mixed Layer Depth Climatology (monthly, 2°) (de Boyer Montégut et al., 2004). Near-surface ocean currents are derived from the NASA Ocean Surface Current Analyses Real-Time version 1 (OSCAR, 1993–2018, pentad, 0.33°) (Bonjean & Lagerloef, 2002). The eastern continental shelf of Australia is highlighted using the 100-m isobath, which is derived from the ETOPO 1 Arc-Minute Global Relief Model (ETOPO1, 1/60°) (Amante & Eakins, 2009) (Figure 1). All of the above data sets are freely and publicly available online; links to the data are provided in the Data Availability Statement found at the end of this paper.

An ocean mixed layer heat budget analysis is calculated for the GBR region (the domain of which is identified in Figure 1), which can be written as follows:

$$\partial T/\partial t = Q_{net}/\rho\, C_p\, h - \mathbf{V}\cdot\nabla T + K\ \nabla^2 T \quad (1)$$

where T is the mixed layer temperature, Q_{net} is the sum of radiative (net surface shortwave and longwave) and turbulent (latent and sensible) heat fluxes less penetrative radiation Q_{pen} (shortwave radiation penetrating through the bottom of the mixed layer), ρ is a mean seawater density (1,025 kg m^{-3}), C_p is the specific heat capacity of seawater (3,850 J kg^{-1} K^{-1}), h is the seasonally varying climatological

mixed layer depth, $-\mathbf{V}\cdot\nabla T$ is temperature advection, and $K\nabla^2 T$ is eddy diffusion. In the budget calculations here, only horizontal temperature advection and eddy diffusion are computed directly; vertical advection, entrainment, and vertical eddy diffusion may be considered the residual. Surface radiative fluxes Q_{rad} are derived from TropFlux and turbulent fluxes Q_{turb} from OAFlux. All four surface fluxes comprising Q_{net} may also be derived from ERA5. For the main results, the simple average of TropFlux +OAFlux and ERA5 is presented; single-data set heat budget calculations are included in the supporting information. Penetrative radiation Q_{pen} is calculated as in Dong and Kelly (2004), after Paulson and Simpson (1977), for water Type 1B (Jerlov, 1968) using mixed layer depth climatology of de Boyer Montégut et al. (2004)). Horizontal advection is calculated using OSCAR currents and OIv2 SST after taking monthly means of the pentad velocity and daily SST fields. A horizontal eddy diffusivity K of 2,000 m^2/s is used, consistent with several previous studies (e.g., Dong & Kelly, 2004; Marshall et al., 2006). All terms on the right-hand side of the heat budget equation 1 are calculated using total variables, after which anomalous terms are calculated (mean seasonal cycle removed) for appropriate comparison with the time evolution of SST anomalies. A monthly rate of change of mixed layer temperature anomaly at every location $\partial T/\partial t$ is calculated as the total change in SST anomaly from the first to the last day of each month using the daily, high-resolution SST (OIv2) following a 15 day low-pass filter to remove high-frequency noise, rendering it appropriate for quantitative, in-phase comparisons with the various heat budget terms described above.

The calculated mixed layer heat budget does not fully close (Figure S5), which is expected given observational uncertainties, use of climatological mixed layer depth, use of low-frequency (monthly mean) variables, use of "surface" quantities for some variables (e.g., SST), use of a relatively coarse ocean velocity data product (0.33° is not fine enough to resolve currents navigating *within* reef systems), and neglect of vertical advection and mixing as noted above. During the time period of interest, monthly residuals are on the order of 0.3°C/month and, more importantly, are uncorrelated ($r^2 = 0.08$) with $\partial T/\partial t$. Among the sources of potential uncertainty in the heat budget calculations, those introduced by the use of climatological (rather than interannually varying) mixed layer depth may be particularly substantial. An estimate of this source of uncertainty is given by repeating the calculations, in Monte Carlo style (10^5 times), using mixed layer depths drawn randomly from a normal distribution of values with the same mean and standard deviation as the climatology (36.8 and 14.4 m, respectively, range [10, 100] enforced). The results of these uncertainty estimates, as concerning two of the major results, are noted in the following section and illustrated in Figure S6.

3. Results

Satellite observations of within-month SST anomaly change ($\partial T/\partial t$) in the GBR region show that the SST anomalies in 2016 arose in two distinct pulses—one beginning in January (0.83°C/month) and another beginning in May (0.42°C/month) (Figure 2). The ocean mixed layer heat budget analysis for the GBR region indicates that $\partial T/\partial t$ is well explained by net surface heat fluxes (Q_{net}) throughout this time period, while horizontal advection and diffusion (AD) contributed negligibly until near the end of the period. Breaking Q_{net} into radiative (Q_{rad}) and turbulent (Q_{turb}) heat fluxes further reveals that the first warming pulse is explained primarily by Q_{rad}, and the second pulse is explained by Q_{turb} (~80% of which was contributed by latent heat flux; not shown). Based on the estimated uncertainty on the calculated $\partial T/\partial t$ (Q_{rad}) in January and $\partial T/\partial t$ (Q_{turb}) in May arising from the use of climatological mixed layer depth (Figure S6), it is extremely unlikely that they would not have emerged as the dominant heat budget terms during those months regardless of mixed layer depth anomalies. These results are also not critically sensitive to whether the surface flux calculations are based on TropFlux, OAFlux, ERA5, or combinations thereof (Figures S2 and S3). While the above heat budget calculations begin to explain the temporal evolution of SST anomaly in the GBR region in 2016, they do not explain why the warming was so concentrated along the east coast of Queensland during the latter stages of the marine heat wave. The majority of the continental shelf is at roughly 50-m depth, which is similar to the mixed layer depth h across the rest of the northern Coral Sea, so a simple argument like "shallower water warms faster given the same Q_{net} anomalies" is insufficient. Let us take a broader view of the climatic forcings that can operate through surface fluxes Q_{rad} and Q_{turb}.

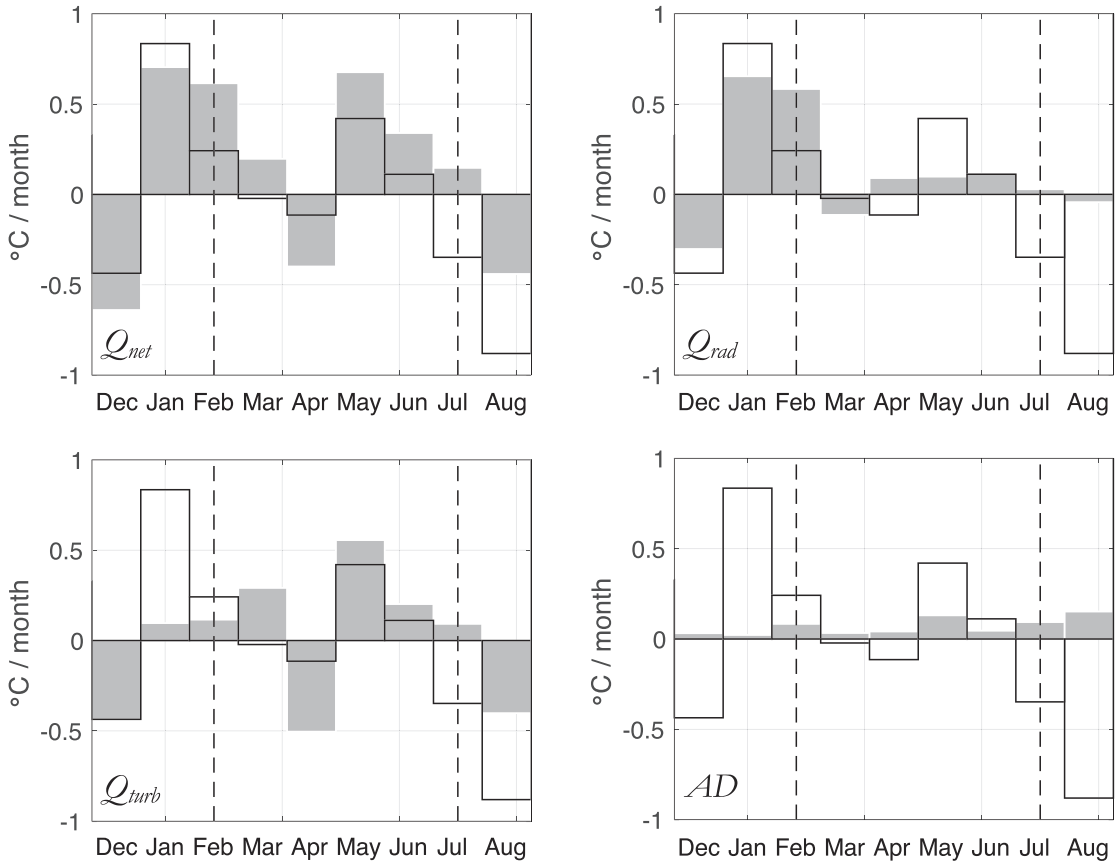

FIGURE 2. Ocean mixed layer heat budget analysis for the GBR region from December 2015 through August 2016. Monthly net surface heat flux (including penetrative radiation Q_{net}), radiative heat flux (Q_{rad}, sum of net surface shortwave and longwave radiation), turbulent heat flux (Q_{turb}, sum of surface latent and sensible heat fluxes), and horizontal temperature advection and diffusion (AD) anomalies are calculated and expressed in terms of $\partial T/\partial t$ (°C/month) using a mean seawater density ρ (1,025 kg m^{-3}), specific heat capacity C_p (3,850 J kg^{-1} K^{-1}), and seasonally varying climatological mixed layer depth h. Open bars, repeated in each panel, represent the total, observed $\partial T/\partial t$ across each month. The vertical dashed lines mark February through July, the period of the warm SST anomaly in the GBR region indicated in Figure 1. Surface fluxes derived from the average of TropFlux (for Q_{rad}) and WHOI OAFlux (for Q_{turb}) and ERA5 for both Q_{rad} and Q_{turb}. See supporting information for single-data set heat budget calculations.

An obvious candidate for modulating Q_{rad} over the tropical oceans is cloud cover (as they block solar radiation and reduce the net surface longwave radiation). Examination of total cloud cover anomalies in the northwestern Coral Sea during this period (Figure 3) confirms that the initial warming pulse and the spikes in Q_{net} and Q_{rad} were driven in part by an anomalous reduction in cloud cover by over 30% in January into February leading to increased solar radiation, consistent with previous reanalysis estimates (Benthuysen et al., 2018). Neither this cloud cover anomaly nor the resulting SST anomaly was enhanced along the coast. However, turning to surface air temperature reveals a strong (>3°C) terrestrial heat wave developing over southeastern Australia near Melbourne in March and propagating northeastward into Queensland by April, consistent with the record warm autumn reported by the Australian Government (Bureau of Meteorology, 2016). In May and June—exactly when the second warming pulse and spikes in Q_{net} and Q_{turb} were observed—the heat wave spilled across the Queensland coastline, which modulated the turbulent heat fluxes preferentially over the continental shelf and further warmed SST in the GBR region. The terrestrial heat wave was not only substantial in areal extent, but the warm air temperature anomalies also extended into the middle troposphere even after crossing the coastline (see daily animation provided in the Movie S1). A simple, back-of-the-envelope calculation of sensible heat flux Q_{SH} using the bulk formula

$$Q_{SH}=\rho\, C_P\, C_{SH}\, W\, \Delta T \tag{2}$$

demonstrates that the terrestrial heat wave, upon crossing the coastline, was sufficient to explain the

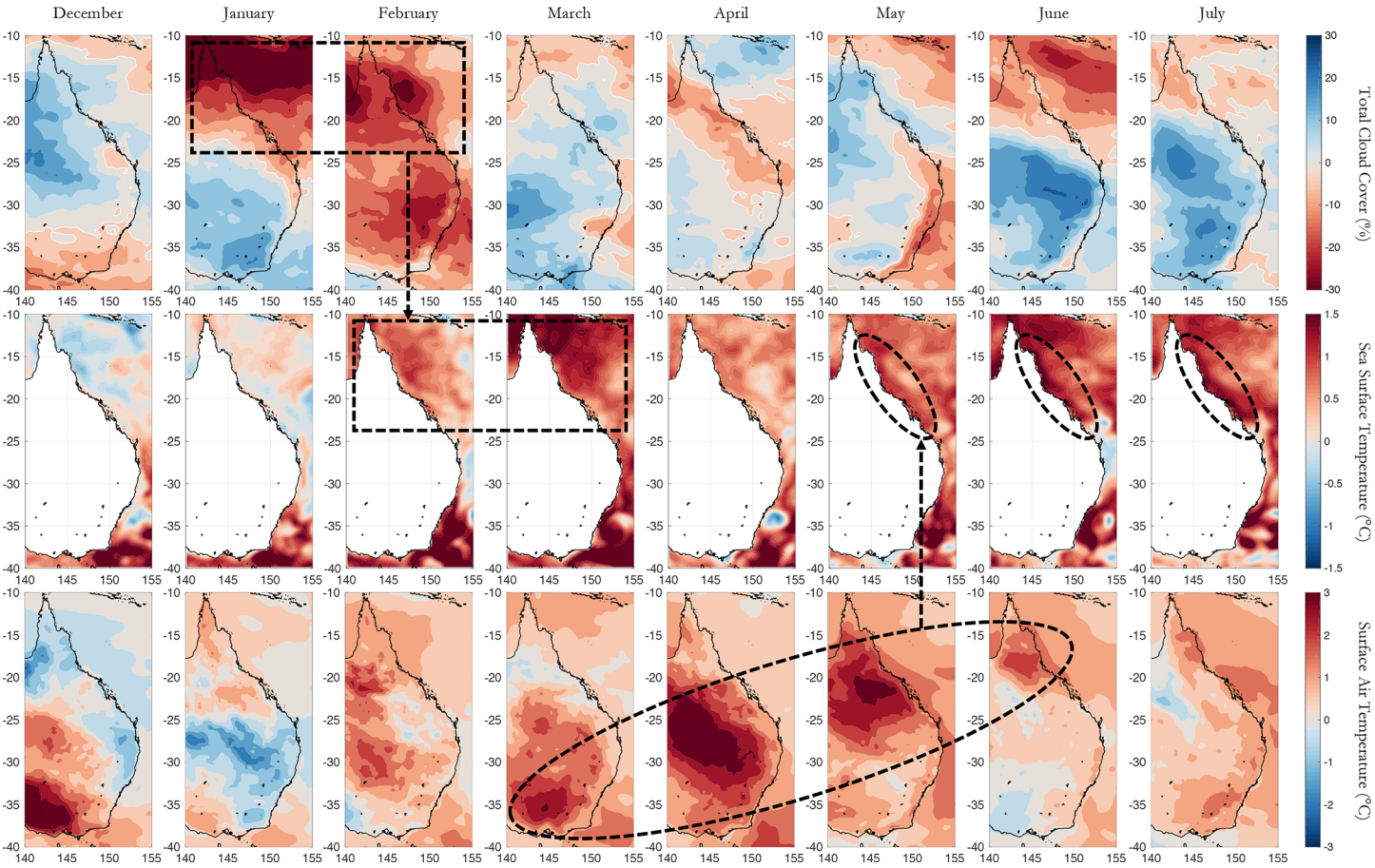

FIGURE 3. Monthly total cloud cover (%, top row), SST (°C, middle row), and surface air temperature (T_{2m}, °C, bottom row) anomalies from ERA5, NOAA OIv2, and ERA5, respectively, spanning December 2015 through July 2016. Base period 1982–2018. Note the different color scales for SST and T_{2m} anomalies. Black dashed boxes, ellipses, and arrows aid the accompanying discussion in the main text.

turbulent heat flux anomaly (which was sufficient to explain the observed SST warming; Figure 2). Examination of ERA5 fields along with observed SSTs from April 2016 (Figure S7) indicates that reasonable values for near-surface wind speed W and air-sea temperate difference ΔT (SST minus 2-m air temperature) near the GBR were 9 m/s and 1.5°C, respectively, prior to the arrival of the atmospheric anomaly. With nominal values of air density ρ (1.2 kg m^{-3}), specific heat capacity of air C_P (1,000 J kg^{-1} K^{-1}), and nondimensional bulk transfer coefficient for the transfer of sensible heat C_{SH} (1.5×10^{-3}), the estimated Q_{SH} over the GBR in April 2016 was +24 W/m^2 (out of the ocean). Imposing, say, a 2°C air temperature anomaly under these conditions yields a new Q_{SH} of −8 W/m^2 (*into* the ocean) or a difference in heat flux into the ocean of +32 W/m^2. The effect of this surface heat flux anomaly on the ocean mixed heat budget $\partial T/\partial t$ can be calculated simply by dividing by $\rho C_P h$ (with ρ and C_P for seawater), yielding 0.43°C/month for h = 50 m (or 0.21–0.85°C/month for doubling and halving of h). These numbers are remarkably close to those from the actual heat budget results in May 2016 (Figure 2). Despite the result that the majority of the Q_{turb} anomaly in May 2016 was accounted for by latent heat flux, the terrestrial heat wave itself was not particularly humid—until it crossed the coastline. Therefore, it is likely that the initial warming was driven by sensible heat flux as diagnosed above, allowing further warming through reduced evaporative flux due to a moistened boundary layer.

It was neither a random coincidence that the GBR warming and mass bleaching event of 2016 occurred following a significant El Niño event nor that it occurred during the decade in which the atmospheric concentration of carbon dioxide passed 400 ppm. What were the specific roles of ENSO and anthropogenic global warming? The reduced cloud cover across the northern Coral Sea is qualitatively consistent with the

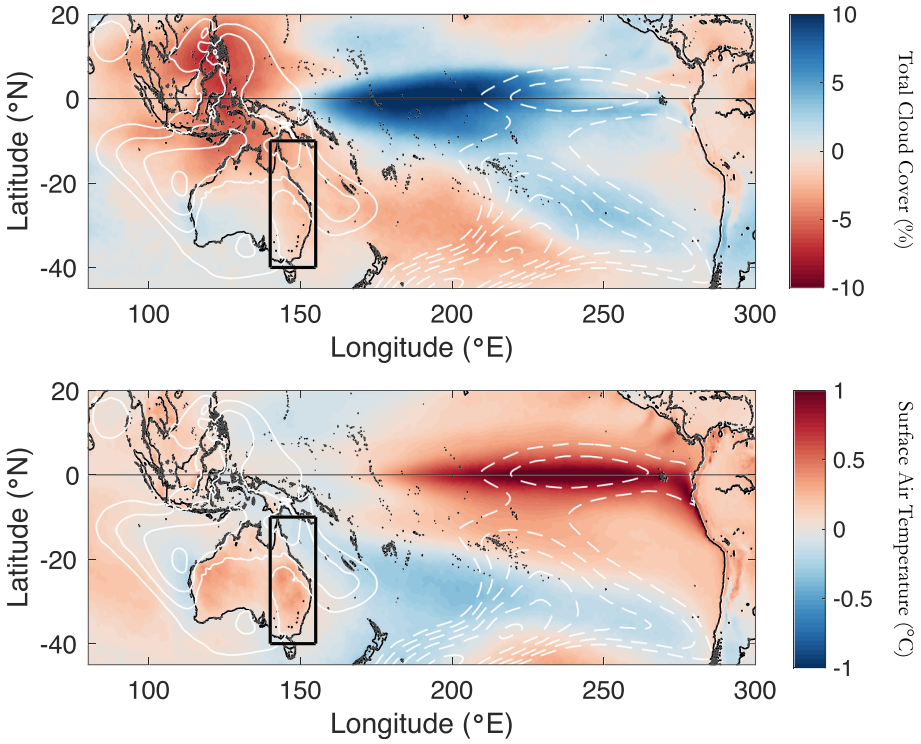

FIGURE 4. Linear regression of monthly total cloud cover (top) and surface air temperature anomalies (T_{2m}, bottom) onto the NINO3.4 index over 1982–2018. Units are %/σ and °C/σ, respectively; the standard deviation (σ) of the NINO3.4 index is 0.96 °C. Also shown in dashed contours is the linear regression of monthly SLP anomalies onto the NINO3.4 index (mb/σ, contoured every 0.1 with contours within $\pm$0.5 omitted for clarity). For context, the black box over eastern Australia and the Coral Sea mark the domain of all maps shown in Figure 3. All three spatial fields from ERA5.

typical, observed pattern of global cloud cover anomalies during El Niño events (Figure 4). During El Niño events, convection (and associated cloud cover) over the tropical Pacific Ocean tightens meridionally and shifts eastward toward the central Pacific (where SST anomalies are large, but the background SST is also warm enough to support deep convection). This equatorward and eastward shift of rainfall brings clear skies and more solar radiation to the Indonesia region and to where the South Pacific Convergence Zone is typically anchored including the northern Coral Sea. Noting that the 2015/2016 El Niño was a 3σ anomaly, the field regression of cloud cover onto ENSO suggests that El Niño contributed approximately one third of the total observed negative cloud cover anomaly over the GBR during the first 2 months of 2016 (~30%). Interestingly, El Niño also typically leads to warm surface air temperature anomalies over Australia, despite the surrounding oceans being slightly cooler (Figure 4). However, this teleconnection to Australia's surface air temperature is only ~0.3°C/σ, so ENSO can only explain up to one third of the >3°C terrestrial heat wave observed over eastern Australia that played a critical role in extending and amplifying the GBR warming in austral autumn 2016.

Meanwhile, surface air temperatures over eastern Australia and SST in the GBR have been warming consistently since 1880 and especially over the past several decades (Figure S4), as expected given the steady rise of greenhouse gas concentrations since the beginning of the Industrial Revolution (IPCC, 2014). A crude estimate of the contribution of the long-term trends in these variables to reaching the observed magnitudes of their anomalies at the height of the 2016 event can be made by detrending their records and placing the 2016 anomalies in the context of the resulting distributions (Figure 5). In the absence of long-term warming signals, large but not unprecedented short-term anomalies of air temperature over eastern Australia and SST in the northwestern Coral Sea would still have occurred in 2016. The superposition of global warming (~1°C in air temperature over eastern Australia and ~0.5°C in SST in the northwestern Coral Sea by 2016) onto those interannual anomalies clearly elevated (by over 50%) their overall magnitudes well beyond the range of observed, natural variability present in a world free of anthropogenic carbon emissions.

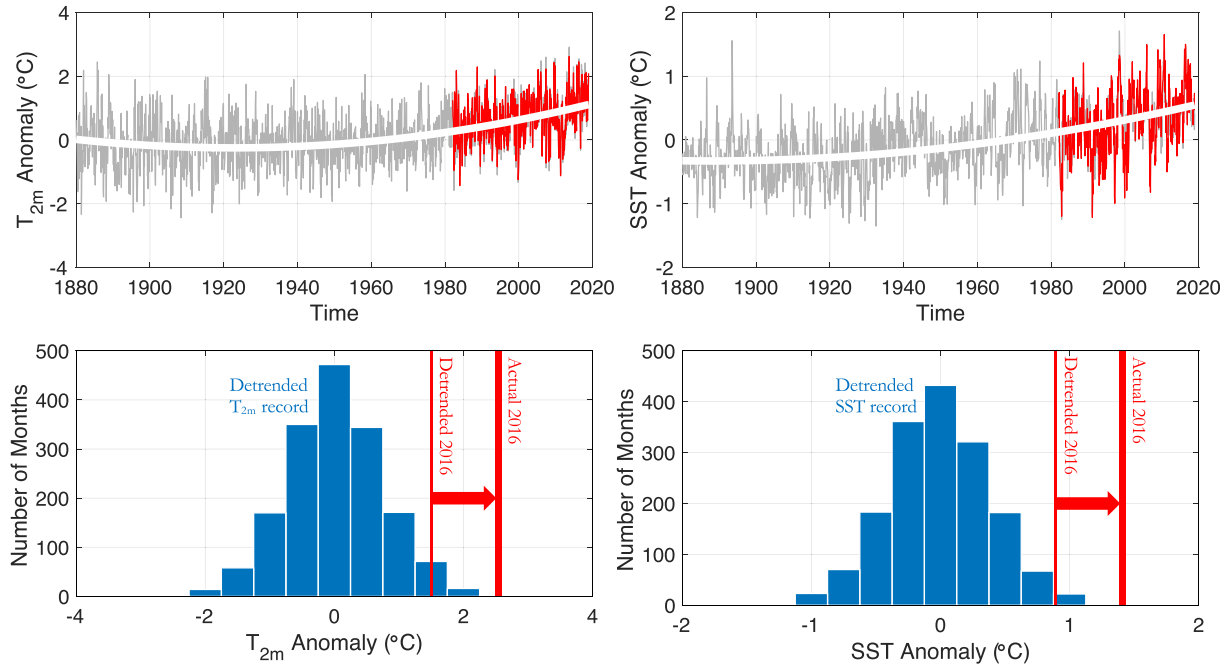

FIGURE 5. Monthly time series of surface air temperature anomaly (T_{2m}, °C) over eastern Australia (averaged over domain marked in Figure S4) from NASA GISTEMP (gray) and ERA5 (red) with a second-order (quadratic) polynomial fit to represent the long-term trend (top left). As in top left but for SST anomaly in the northwestern Coral Sea from HadISST and NOAA OIv2 (top right). The bottom plots are histograms of the corresponding detrended (by removing the quadratic trendlines) long-term records. The thin (thick) red lines indicate the peak anomalies in 2016 in the detrended (full) records.

4. Summary and Discussion

Analysis of the 2016 marine heat wave that led to severe bleaching and mortality on the GBR was presented, including quantitative diagnosis via the ocean mixed layer heat budget drawing from a diverse range of satellite and other observationally constrained data products. The warming observed at the GBR in 2016 was shown to be a two-step process. First, the 2015/2016 El Niño shifted the distribution of clouds away from the northern Coral Sea, making way for surface warming by solar radiation. Just as this initial SST anomaly began to wane, a terrestrial heat wave over eastern Australia arrived at the Queensland coastline, serving to amplify and extend the SST warming at the GBR through turbulent heat flux. This mechanism for extending the duration of the 2016 marine heat wave in the GBR is quite different than the one proposed by Wolanski et al. (2017), who employed particle and hydrodynamic modeling to argue for a dominant role of changes in coastal ocean currents. While both may have contributed—especially in the northern sector of the GBR—turbulent fluxes alone are sufficient to quantitatively explain the observed warming pulse in May and June 2016 across the GBR. Wolanski et al. (2017) concluded that "The fate of the Great Barrier Reef is thus controlled by the oceanography of surrounding seas," but the analysis presented here suggests that the meteorology of surrounding land, as well as remotely forced regional atmospheric circulation anomalies, dominated the 2016 marine heat wave in the GBR. Anthropogenic climate change, ongoing since the middle nineteenth century, interfered constructively with the natural variability of Australian surface air temperatures—elevating the probability of extreme terrestrial heat waves through a shifting distribution. Long-term ocean warming has also raised the background SST throughout the western Coral Sea, enabling radiation anomalies associated with modes of natural climate variability like ENSO to raise absolute SSTs to higher levels for longer periods of time. This notion is consistent with Lewis and Mallela (2018), who concluded that global warming was the primary increased *risk factor* for the extreme bleaching in 2016, with a concerning outlook for the frequency of future bleaching events as radiative forcing only becomes stronger. There are thus a multitude of pathways for anthropogenic climate change to exacerbate the threat of short-term thermal anomalies to Earth's most vital coral reef ecosystems.

Data Availability Statement

All data sets used in this study are freely and publicly available online and may be accessed directly as follows. NOAA High-Resolution Blended Analysis of Daily SST and Ice version 2 (https://www.esrl.noaa.gov/psd/data/gridded/data.noaa.oisst.v2.highres.html), Hadley Centre Sea Ice and Sea Surface Temperature version 1 (https://www.metoffice.gov.uk/hadobs/hadisst/), ECMWF Reanalysis version 5 (https://cds.climate.copernicus.eu/#!/search?text=ERA5&type=dataset), NASA GISS Surface Temperature Analysis version 4 (https://data.giss.nasa.gov/gistemp/), INCOIS TropFlux version 1 (https://incois.gov.in/tropflux/data_access.jsp), WHOI Objectively Analyzed Air-Sea Fluxes version 3 (http://oaflux.whoi.edu/data.html), IFREMER Mixed Layer Depth Climatology (http://www.ifremer.fr/cerweb/deboyer/mld/Surface_Mixed_Layer_Depth.php), NASA Ocean Surface Current Analyses Real–Time version 1 (ftp://podaac-ftp.jpl.nasa.gov/allData/oscar/preview/L4/oscar_third_deg), and ETOPO 1 Arc-Minute Global Relief Model (https://www.ngdc.noaa.gov/mgg/global/).

Acknowledgments
The author thanks Dr. Tom DeCarlo and anonymous reviewers for valuable comments on this study. The author also thanks all of the producers of the global, gridded data sets listed in section 22, and the institutional repositories hosting them, including ECMWF, IFREMER, INCOIS, NASA, NOAA, UKMO, and WHOI.

References

Amante, C., & Eakins, B. W. (2009). ETOPO1 1 arc-minute global relief model: Procedures, data sources and analysis. NOAA technical memorandum NESDIS NGDC-24. National geophysical data center, NOAA. https://doi.org/10.7289/V5C8276M

ARC Centre of Excellence Coral Reef Studies (2017). 2016 global coral bleaching: Never a greater need for coral reef research, Annual Report 2016. 91 pp.

Benthuysen, J. A., Oliver, E. C. J., Feng, M., & Marshall, A. G. (2018). Extreme marine warming across tropical Australia during austral summer 2015–2016. *Journal of Geophysical Research: Oceans*, *123*, 1301–1326. https://doi.org/10.1002/2017JC013326

Bonjean, F., & Lagerloef, G. S. E. (2002). Diagnostic model and analysis of the surface currents in the tropical Pacific Ocean. *Journal of Physical Oceanography*, *32*, 2938–2954. https://doi.org/10.1175/1520-0485(2002)032<2938:DMAAOT>2.0.CO;2

Bureau of Meteorology (2016). Special Climate Statement 56—Australia's warmest autumn on record. Issued 1 June 2016. Published by the Bureau of Meteorology of the Australian Government. 21 pp. http://www.bom.gov.au/climate/current/statements/scs56.pdf

de Boyer Montégut, C., Madec, G., Fischer, A. S., Lazar, A., & Iudicone, D. (2004). Mixed layer depth over the global ocean: An examination of profile data and a profile–based climatology. *Journal of Geophysical Research*, *109*, C12003. https://doi.org/10.1029/2004JC002378

Dong, S., & Kelly, K. A. (2004). Heat budget in the Gulf Stream region: The importance of heat storage and advection. *Journal of Physical Oceanography*, *34*, 1214–1231.

Great Barrier Reef Marine Park Authority (2017). Final report: 2016 coral bleaching event on the Great Barrier Reef, GBRMPA, Townsville.

Hersbach, H., Bell, W., Berrisford, P., Horányi, A., Sabater, J. M., Nicolas, J., et al. (2019). Global reanalysis: Goodbye ERA-interim, hello ERA5. *ECMWF Newsletter*, *159*, 17–24. https://doi.org/10.21957/vf291hehd7

Hughes, T. P., Anderson, K. D., Connolly, S. R., Heron, S. F., Kerry, J. T., Lough, J. M., et al. (2018). Spatial and temporal patterns of mass bleaching of corals in the Anthropocene. *Science*, *359*(6371), 80–83. https://doi.org/10.1126/science.aan8048

Hughes, T. P., Kerry, J. T., Álvarez-Noriega, M., Álvarez-Romero, J. G., Anderson, K. D., Baird, A. H., et al. (2017). Global warming and recurrent mass bleaching of corals. *Nature*, *543*(7645), 373–377. https://doi.org/10.1038/nature21707

Hughes, T. P., Kerry, J. T., Baird, A. H., Connolly, S. R., Dietzel, A., Eakin, C. M., et al. (2018). Global warming transforms coral reef assemblages. *Nature*, *556*(7702), 492–496. https://doi.org/10.1038/s41586-018-0041-2

IPCC (2014). *Climate change 2013—The physical science basis: Working group I contribution to the fifth assessment report of the intergovernmental panel on climate change*. Cambridge: Cambridge University Press.

Jerlov, N. G. (1968). *Optical oceanography* (p. 199). New York: Elsevier.

Karnauskas, K. B. (2013). Can we distinguish canonical El Niño from Modoki? *Geophysical Research Letters*, *40*, 5246–5251. https://doi.org/10.1002/grl.51007

Lenssen, N., Schmidt, G., Hansen, J., Menne, M., Persin, A., Ruedy, R., & Zyss, D. (2019). Improvements in the GISTEMP uncertainty model. *Journal of Geophysical Research: Atmospheres*, *124*, 6307–6326. https://doi.org/10.1029/2018JD029522

Lewis, S. C., & Mallela, J. (2018). A multifactor risk analysis of the record 2016 Great Barrier Reef bleaching. *Bulletin of the American Meteorological Society*, *99*, S144–S149. https://doi.org/10.1175/BAMS-D-17-0074.1

Lough, J. M. (1994). Climate variation and El Niño–Southern Oscillation events on the Great Barrier Reef: 1958 to 1987. *Coral Reefs*, *13*(3), 181–185.

Marshall, J., Shuckburgh, E., Jones, H., & Hill, C. (2006). Estimates and implications of surface eddy diffusivity in the Southern Ocean derived from tracer transport. *Journal of Physical Oceanography*, *36*, 1806–1821.

Paulson, C., & Simpson, J. (1977). Irradiance measurements in upper ocean. *Journal of Physical Oceanography*, *7*, 952–956. https://doi.org/10.1175/1520-0485(1977)007<0952:IMITUO>2.0.CO;2

Praveen Kumar, B., Vialard, J., Lengaigne, M., Murty, V. S. N., & McPhaden, M. J. (2012). TropFlux: Air-sea fluxes for the global tropical oceans—Description and evaluation. *Climate Dynamics*, *38*, 1521–1543. https://doi.org/10.1007/s00382-011-1115-0

Rayner, N. A., Parker, D. E., Horton, E. B., Folland, C. K., Alexander, L. V., Rowell, D. P., et al. (2003). Global analyses of sea surface temperature, sea ice, and night marine air temperature since the late nineteenth century. *Journal of Geophysical Research*, *108*(D14), 4407. https://doi.org/10.1029/2002JD002670

Reynolds, R. W., Rayner, N. A., Smith, T. M., Stokes, D. C., & Wang, W. (2002). An improved in situ and satellite SST analysis for climate. *Journal of Climate*, *15*, 1609–1625. https://doi.org/10.1175/1520-0442(2002)015<1609:AIISAS>2.0.CO;2

Stuart-Smith, R. D., Brown, C. J., Ceccarelli, D. M., & Edgar, G. J. (2018). Ecosystem restructuring along the Great Barrier Reef following mass coral bleaching. *Nature*, *560*, 92–96. https://doi.org/10.1038/s41586-018-0359-9

Wolanski, E., Andutta, F., Deleersnijder, E., Li, Y., & Thomas, C. J. (2017). The Gulf of Carpentaria heated Torres Strait and the Northern Great Barrier Reef during the 2016 mass coral bleaching event. *Estuarine, Coastal and Shelf Science*, *194*, 172–181. https://doi.org/10.1016/j.ecss.2017.06.018

Yu, L. S., & Weller, R. A. (2007). Objectively analyzed air-sea heat fluxes for the global ice-free oceans (1981–2005). *Bulletin of the American Meteorological Society*, *88*(4), 527–539. https://doi.org/10.1175/BAMS-88-4-527

Zhang, N., Feng, M., Hendon, H. H., Hobday, A. J., & Zinke, J. (2017). Opposite polarities of ENSO drive distinct patterns of coral bleaching potentials in the southeast Indian Ocean. *Scientific Reports*, *7*(1), 1–10.